Nanoscale

PAPER

Cite this: *Nanoscale*, 2019, **11**, 20614

Nacre-inspired moisture-responsive graphene actuators with robustness and self-healing properties†

Jiang-Wei Mao,[a] Zhao-Di Chen,[a] Dong-Dong Han,[a] Jia-Nan Ma,[a] Yong-Lai Zhang *[a] and Hong-Bo Sun [a,b]

Received 1st August 2019,
Accepted 26th September 2019
DOI: 10.1039/c9nr06579b
rsc.li/nanoscale

Moisture-responsive actuators based on graphene oxide (GO) have attracted intensive research interest in recent years. However, current GO actuators suffer from low mechanical strength. Inspired by the robustness of nacre's structure, moisture-responsive actuators with high mechanical strength and self-healing properties were successfully developed based on GO and cellulose fiber (CF) hybrids. The hybrid paper demonstrated significantly improved tensile strength, ∼20 times higher than that of pure GO paper, and self-healing properties. A broken paper can be well cured under moist conditions, and the mechanical properties of the self-healed hybrid paper can still maintain similar tensile strength to the pristine one. After controllable ultraviolet light photoreduction treatment, a hybrid paper with a photoreduction gradient along the normal direction was prepared, which can act as a moisture-responsive actuator. A maximum bending curvature of ∼1.48 cm^{-1} can be achieved under high relative humidity (RH = 97%). As a proof-of-concept, a butterfly-like actuator that can deform itself with moisture actuation was demonstrated. Our approach may pave a new way for designing robust and self-healable graphene actuators.

Introduction

Actuators are able to change their shapes rapidly and reversibly under a variety of stimuli including light,[1] thermal,[2,3] electricity,[4] humidity,[5,6] and others.[7–9] To date, actuators have aroused great interest since they have revealed broad potential in cutting-edge applications including flexible robots,[10,11] biological devices,[12,13] micro-electromechanical systems,[14,15] microfluidic chips,[16–18] *etc*. To develop actuators, stimulus-responsive structures (*e.g.*, bi-/multi-layer materials) have been well studied, since they permit large-scale and complex deformations.[19] Moreover, taking advantage of the stress mismatch between different material layers under external stimuli, actuation of these bi-/multi-layer structures is usually controllable. However, to achieve a fast and reversible response, bimorph actuators usually have very thin structures and thus suffer from poor mechanical strength. Currently, it is still challenging to develop bimorph actuators with reasonable robustness and self-healing properties to improve the environmental adaptability.

Recently, graphene has been widely studied due to its excellent physical and chemical properties, such as flexibility, extraordinary mechanical strength, large surface area, and others.[20–24] As an important derivative of graphene, graphene oxide (GO) possesses abundant oxygen-containing functional groups (OCGs) on its basal plane and edges, which are very sensitive to water molecules. Thus, GO has been widely used in the development of humidity sensors, actuators, and water vapor power generation devices.[25–29] Various bio-inspired nanostructures have been fabricated based on GO *via* laser nanostructuring or indirect laser-assisted pattern transfer.[30] Especially, in the case of moisture-responsive actuators, Qu *et al.* and others have successfully prepared GO-based moisture-responsive fibers and papers *via* chemical and photoreduction methods.[31–33] However, these GO actuators still suffer from poor mechanical strength, especially after reduction treatment, which limits their applications significantly.

In this paper, inspired by the layered nacre structure, GO and cellulose fiber (CF) hybrid papers with improved stiffness were prepared. The CFs that contain abundant hydroxyl

[a]*State Key Laboratory of Integrated Optoelectronics, College of Electronic Science and Engineering, Jilin University, 2699 Qianjin Street, Changchun 130012, China. E-mail: yonglaizhang@jlu.edu.cn*
[b]*State Key Lab of Precision Measurement Technology and Instruments, Department of Precision Instrument, Tsinghua University, Haidian, Beijing 100084, China*

†Electronic supplementary information (ESI) available. See DOI: 10.1039/c9nr06579b

groups show a strong interaction with GO (hydrogen bonds), which promotes their tensile strength significantly in a similar way to nacre. Unilateral photoreduction of the hybrid paper can make it suitable for moisture actuation, since the OCG gradient can form along the normal direction upon controllable photoreduction. Moreover, the GO and CF hybrid papers show self-healing ability upon exposure to moisture/air. Furthermore, since the addition of fibers facilitates the transmission of water molecules, the moisture responsiveness of the actuators can be improved. As a proof-of-concept, a humidity-responsive butterfly based on the unilaterally reduced GO and CF papers was demonstrated.

Results and discussion

It is well known that nacre shows outstanding mechanical strength (Fig. 1a).[34] A cross-section scanning electron microscopy (SEM) image of nacre shows a highly stacked "brick-and-mortar" nanostructure, in which brittle calcium carbonate platelets bind to a biopolymer layer (Fig. 1b and c). Inspired by the nanostructure of natural nacre, a GO-CF hybrid paper was assembled in a similar way (Fig. 1d). First, the GO aqueous solution prepared *via* Hummers' method (Fig. S1a) was mixed with a CF solution prepared using napkin pieces (Fig. S1b†). Then, the GO and CF mixture (in a volume ratio of 3 : 1) was cast into a plastic Petri dish and dried under air. After this, the hybrid paper was formed, and it was peeled off for further use. In this hybrid paper, GO was employed as the basic building block. The CF that is made of 7000 to 10 000 glucose molecules,[35] linked by glycosidic chains, can bind to GO sheets *via* hydrogen bonds (Fig. 1e and f). The as-formed hybrid structure is similar to nacre. The interaction between GO and CF was monitored using IR spectra (Fig. S2†).[36–39] The characteristic vibration bands of GO were observed such as ν_{phenolic} at 1247 cm^{-1} and $\nu_{C\text{–}O}$ at 1080 cm^{-1}. Due to the formation of hydrogen bonds between GO sheets and the CF, a widening and downshift of the peak (centered at ~3410 cm^{-1}) was detected. In addition, UV irradiation was used to trigger the photoreduction of GO (RGO). UV irradiation of GO is found to be a highly controllable protocol to trigger the photoreduction of GO. Under UV irradiation, some of the OCGs on GO sheets can be removed in a controlled manner. The unilateral UV reduction of GO papers was employed for a facile and large-scale production of RGO/GO bilayer papers.[5] By controlling the photoreduction degree, a gradient RGO-CF/GO-CF film was fabricated (Fig. 1g). Due to the removal of OCGs, the upper stacked GO sheets were exfoliated and the unexposed side retains the stacked structure (Fig. 1h). From the SEM image of the GO-CF, the CF and wrinkles of GO are clearly seen (Fig. 1i).

Fig. 2 shows the self-healing process of a GO-CF paper. It can repair the physical damage automatically under moist conditions. To observe the moisture-triggered self-healing behaviour, a square GO-CF was cut into two pieces (Fig. 2a), and the broken surfaces were exposed to a humidifier for 10 min. Then, these two pieces were able to rejoin autonomously (Fig. 2b). Fig. 2c shows the SEM image of a cut GO-CF paper

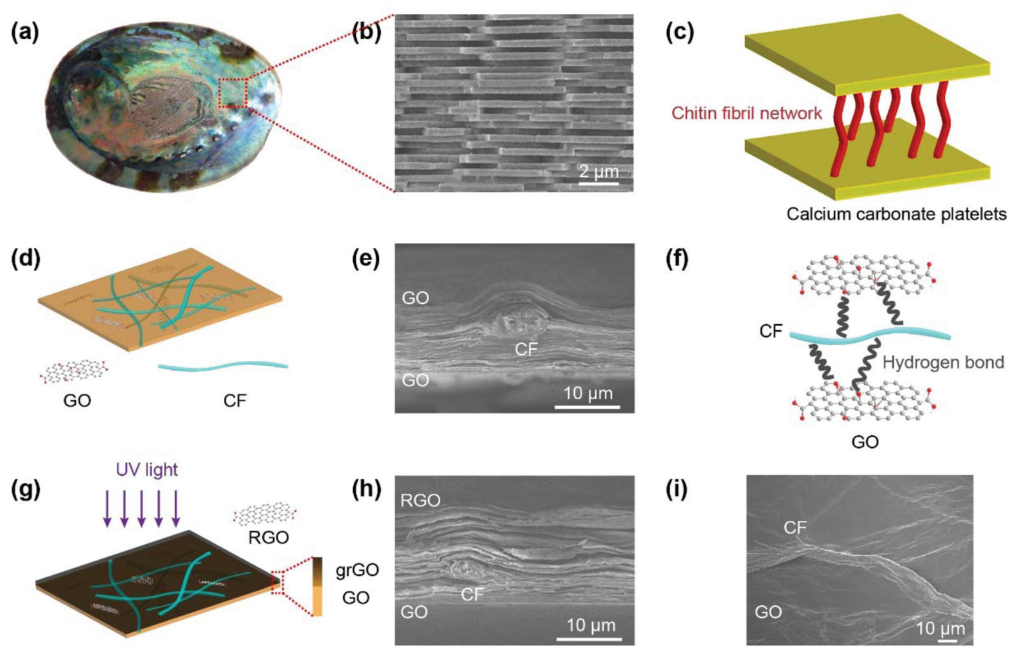

Fig. 1 (a) Photograph of an abalone shell. (b) SEM images of the cross-section of nacre. (c) Schematic diagram of a nacre model. (d) Schematic diagram of the GO-CF hybrid paper. (e) Cross-sectional SEM image of a GO layered structure with CF. (f) Schematic diagram of the interaction between GO and CF. (g) Schematic illustration of the UV irradiation-induced gradient structure. (h) Cross-sectional SEM image of the hybrid paper with a photoreduction gradient. (i) SEM image of the surface of the hybrid paper.

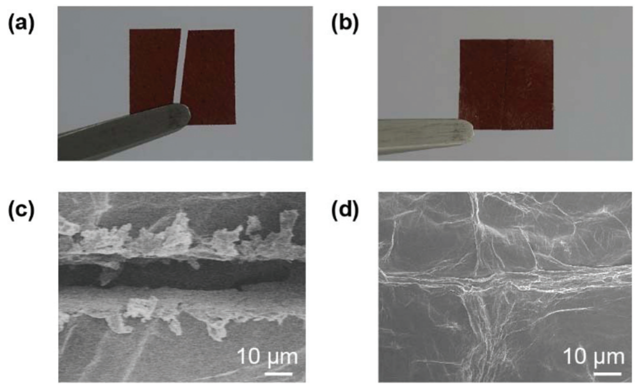

Fig. 2 Photographs of the GO-CF hybrid paper before (a) and after (b) moisture-triggered self-healing. (b) SEM images of the incision on the surface of the GO-CF hybrid paper before (c) and after (d) moisture-triggered self-healing.

with an obvious wound. After the GO-CF paper is self-healed, the scar can be hardly observed on the surface (Fig. 2d).

Fig. 3a and b present the tensile properties of GO, RGO/GO, GO-CF, RGO-CF/GO-CF, and the self-healed GO-CF. Loading of CF into the GO film improved the mechanical strength. The GO paper has a tensile strength of 33.34 MPa, with a maximum elongation at break of ~1.5% (Fig. 3a). In the presence of CF, the tensile strength of the hybrid paper increased abruptly to 696 MPa, about 20 times that of GO without CF (Fig. 3b). For comparison, we also measured the tensile strength of the CF paper, which is only ~6 MPa (Fig. S3†). This proved that the improvement in mechanical tensile strength can be attributed to the addition of CF and the strong interaction between GO nanosheets and the CF (Fig. 1d and f). Meanwhile, the tensile strength of the self-healed hybrid paper was also studied (Fig. 3b). Interestingly, the tensile strength of the healed GO-CF slightly decreased to 600 MPa and the maximum elongation at break increased to ~2%. After the healing treatment, tensile properties almost maintained the same grade.

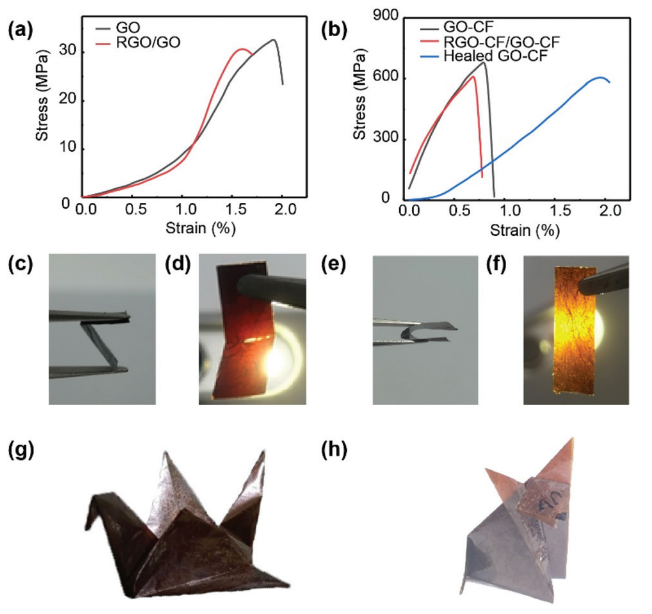

Fig. 3 (a) The stress–strain curves of GO and RGO/GO. (b) The stress–strain curves of GO-CF, RGO-CF/GO-CF, and the self-healed GO-CF obtained through tensile tests. (c and d) Photographs of the folded RGO/GO bilayer paper and (e and f) the folded RGO-CF/GO-CF bilayer paper. The photograph of an origami crane (g) and fox (h) folded using the GO-CF paper.

As shown in Fig. 3c, we folded an RGO/GO bilayer paper. Tiny cracks can be observed under light (Fig. 3d). For comparison, we folded the RGO-CF/GO-CF paper to a larger angle (Fig. 3e). There are no cracks, which suggests better robustness (Fig. 3f). To quantitatively investigate the robustness of these samples, the stress–strain curves of RGO/GO and RGO-CF/GO-CF after folding 2 times and 100 times, respectively, were measured for comparison (Fig. S4†). After folding 2 times, the RGO/GO film was broken and thus the tensile strength was 0 MPa. The RGO-CF/GO-CF paper demonstrated a much better mechanical strength during the folding test. Its strength was 38 MPa after folding 100 times, which is comparable to the pristine RGO/GO paper. For comparison, the tensile strength of different samples is shown in Fig. S5.† Due to the excellent mechanical tensile strength (Table S1†), the GO-CF paper can be employed for origami, such as cranes (Fig. 3g) and foxes (Fig. 3h).

The content of OCGs was further evaluated by X-ray photoelectron spectroscopy (XPS, Fig. 4). The survey spectra of the GO and RGO surfaces show the peaks of C 1s and O 1s at 285 and 532 eV, respectively (Fig. 4a). As compared with GO, the O 1s peak of RGO is significantly reduced and the C 1s peak increased. Based on the atomic percentages, C/O ratios of the

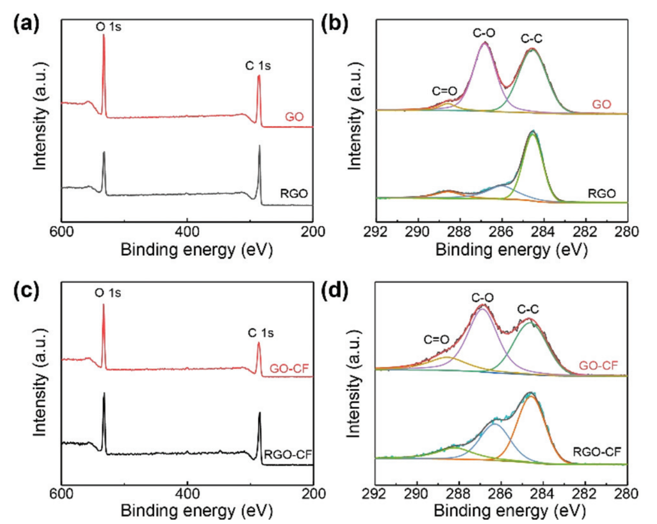

Fig. 4 (a) XPS survey spectra of the not reduced side and the UV processed side of the RGO/GO bilayer paper. (b) C 1s spectra of the GO and RGO sides. (c) The XPS survey spectra of the not reduced side and the UV processed side of the RGO-CF/GO-CF paper. (d) C 1s spectra of the GO-CF and RGO-CF sides.

GO and RGO papers are 2.23 and 3.17, respectively. The C 1s spectra can be deconvoluted into three major peaks with positions of 284.65, 286.9 and 288.6 eV, representing C–C, C–O and C=O, respectively (Fig. 4b). Compared with GO, the C–O bonds of RGO significantly reduced because of the photoreduction process. The C–O and C–C bonds of GO are calculated to be 48% and 44%, respectively, whereas the C–O and C–C bonds of RGO are 23% and 69%, respectively, indicating the decrease of OCG content after UV treatment. The decrease of OCGs can be attributed to the UV photoreduction effect.

Similarly, XPS analysis of the GO-CF and RGO-CF sides of the hybrid paper also indicated the removal of OCGs (Fig. 4c). Compared with the GO-CF side, the O 1s peak of the RGO-CF side is significantly reduced and the C 1s peak increased. Based on the atomic percentages, C/O ratios of the GO-CF and RGO-CF papers are calculated to be 2.15 and 2.76, respectively. The C–O and C–C bonds of the RGO-CF paper are 32% and 58%, respectively. In addition, we also measured the XPS spectra of the CF before and after UV irradiation (Fig. S6†). After UV treatment, the pristine CF almost showed unchanged carbon and oxygen element contents. This result indicated that the decrease of the oxygen signal can be attributed to the photoreduction of GO. By comparing the C 1s spectra of RGO and RGO-CF, more C–O bonds were detected in the RGO-CF paper. This can be ascribed to the presence of CF that cannot be reduced upon UV irradiation.

It is worth noting that the presence of the CF in the GO film can not only improve the stiffness, but also promote the moisture-responsive properties. As we know, the GO paper has a layered nanostructure that can provide nanochannels for water molecule diffusion (Fig. 5a). The addition of CF can create additional micro-channels between the GO sheets (Fig. 5b). The hierarchical micro-nanostructure is quite helpful for water molecule transmission, and thus promotes the moisture-responsive properties. In the moisture actuation tests, the RGO-CF/GO-CF paper exhibits humidity-responsive bending properties due to the anisotropic expansion properties of the two sides. In order to quantitatively study the bending curvature of this RGO-CF/GO-CF paper, we measured the bending curvature of an RGO-CF/GO-CF ribbon (1.5 mm × 15 mm) under different humidity conditions. When the relative humidity (RH) increases from 24% to 97%, its curvature increases from the initial flat state (0 cm^{-1}) to 1.48 cm^{-1} (Fig. 5c). The inset of Fig. 5c shows the side-view images of the ribbon under different humidity conditions. We also measured the response and recovery cycles by switching the relative humidity between 24% and 97% (Fig. 5d). When the humidity increases to 97%, the RGO-CF/GO-CF paper quickly bends to a curvature of 1.48 cm^{-1} within 10 s. It can recover to its original state within 6s, indicating the quick response. Using this moisture-responsive RGO-CF/GO-CF paper, we fabricated a moisture-responsive butterfly through a scissor-cut process. The butterfly was placed on a picture (Fig. 5e and f). We switched the environmental humidity, so that the butterfly could flap its wings (the insets of Fig. 5e and f).

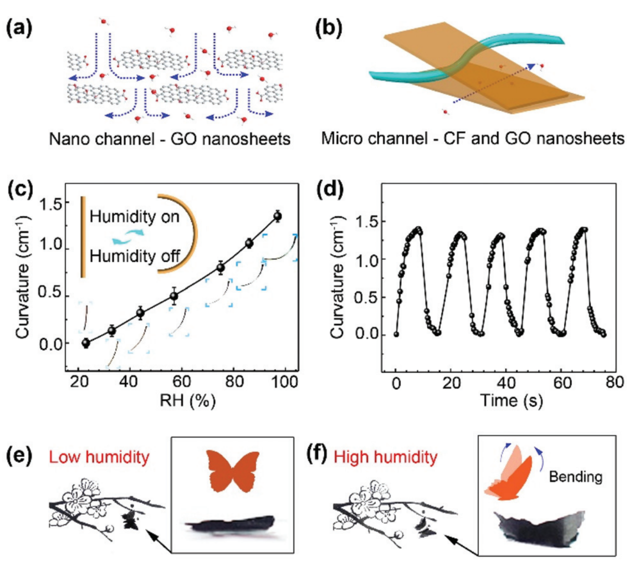

Fig. 5 (a and b) Schematic illustration of nano-/micro-channels for water molecule transmission. (c) The relationship between the bending curvature and relative humidity. (d) Bending curvature of the actuator for multiple cycling changes between RH = 23% and RH = 97%. (e) Photograph of RGO-CF/GO-CF-based butterfly. (f) The moisture-triggered RGO-CF/GO-CF-based butterfly.

Conclusions

In summary, inspired by the robustness of nacre's structure, we demonstrated the preparation of GO and CF hybrid papers with improved mechanical properties and self-healing ability. The hybrid paper exhibited a tensile strength of 696.86 MPa, which is about 20 times higher than that of the GO paper (33.34 Mpa). Similar to GO, the hybrid paper also demonstrated self-healing properties; a broken paper can be well cured upon exposure to moisture due to the re-assembly of GO sheets and the CF. More importantly, the mechanical properties of the self-healed hybrid paper can still maintain high tensile properties, similar to that of the pristine one. Subsequently, we demonstrated the fabrication of humidity-responsive actuators by unilateral UV photoreduction treatment of the hybrid paper. A bending curvature of 1.48 cm^{-1} was achieved when the environmental relative humidity increased from 23% (room condition) to 97%. We deem that the actuators based on our GO and CF hybrid papers may have improved robustness and environmental adaptability.

Experimental

Preparation of GO-CF

First, the GO aqueous solution was prepared *via* Hummers' method. The CF solution was prepared by mixing 0.7602 g of napkin pieces with 150 ml of water and stirring for 24 h. Then, the mixed GO solution and CF solution (in a volume ratio of

3 : 1) was naturally dried in a plastic Petri dish. Finally, the GO-CF paper was peeled off for the further use.

Self-healing of GO-CF

The GO-CF paper was cut into two pieces using a knife and placed closely. Then, a humidifier was used to heal the incision for 10 min.

Ultraviolet light photoreduction of GO-CF

The GO-CF paper was exposed to ultraviolet light for 200 seconds. The target gradient RGO-CF/GO-CF paper was fabricated.

Characterization

The morphology was characterized by using a JEOL-JSM-7500 field-emission scanning electron microscope. X-ray photoelectron spectroscopy (XPS) was performed by using an ESCALAB 250 spectrometer. INSTRON-5869 was used to measure the mechanical properties at a loading rate of 2 mm min^{-1}. A 5 × 25 mm (width × length) strip was used for mechanical testing. Different relative humidity environments were obtained using different saturated salt solutions, including CH_3COOK, $MgCl_2$, KCO_3, NaBr, NaCl, KCl, and K_2SO_4, which yielded approximately 23, 33, 44, 57, 68, 86, and 97% relative humidity (RH). All experiments were performed at room temperature.

Conflicts of interest

There are no conflicts to declare.

Acknowledgements

This work was supported by the National Key Research and Development Program of China, the National Natural Science Foundation of China (NSFC) under Grant No. #2017YFB1104300, #61935008, #61775078, #61590930, and #61905087, and the Scientific and Technological Developing Scheme of Jilin Province No. #20180101061JC.

Notes and references

1 D. Schneidereit, S. Nubler, G. Prolss, B. Reischl, S. Schurmann, O. J. Muller and O. Friedrich, *Light: Sci. Appl.*, 2018, **7**, 79.
2 B. Han, Y.-L. Zhang, Q.-D. Chen and H.-B. Sun, *Adv. Funct. Mater.*, 2018, **28**, 1802235.
3 J. Li, L. Mou, R. Zhang, J. Sun, R. Wang, B. An, H. Chen, K. Inoue, R. Ovalle-Robles and Z. Liu, *Carbon*, 2019, **148**, 487–495.
4 M. Weng, P. Zhou, L. Chen, L. Zhang, W. Zhang, Z. Huang, C. Liu and S. Fan, *Adv. Funct. Mater.*, 2016, **26**, 7244–7253.
5 D.-D. Han, Y. L. Zhang, Y. Liu, Y.-Q. Liu, H.-B. Jiang, B. Han, X.-Y. Fu, H. Ding, H.-L. Xu and H.-B. Sun, *Adv. Funct. Mater.*, 2015, **25**, 4548–4557.
6 Y.-L. Zhang, Y.-Q. Liu, D.-D. Han, J.-N. Ma, D. Wang, X.-B. Li and H.-B. Sun, *Adv. Mater.*, 2019, **31**, 1901585.
7 Z. Sun, S. Du, D. Zhang and W. Song, *React. Funct. Polym.*, 2019, **139**, 102–111.
8 H. J. Lin, S. Y. Zhang, Y. Xiao, C. J. Zhang, J. X. Zhu, J. W. C. Dunlop and J. Y. Yuan, *Macromol. Rapid Commun.*, 2019, **40**, 1800896.
9 Y.-L. Zhang, Y. Tian, H. Wang, Z.-C. Ma, D.-D. Han, L.-G. Niu, Q.-D. Chen and H.-B. Sun, *ACS Nano*, 2019, **13**, 4041–4048.
10 D. Kim, J. I. Kim and Y.-L. Park, *IEEE Robot. Autom. Lett.*, 2019, **4**, 2289–2295.
11 T. Verstraten, R. Furnemont, P. Beckerle, B. Vanderborght and D. Lefeber, *IEEE Robot. Autom. Lett.*, 2019, **4**, 2310–2316.
12 T. Zheng, P. P. S. S. Abadi, J. Seo, B.-H. Cha, B. Miccoli, Y.-C. Li, K. Park, S. Park, S.-J. Choi, R. Bayaniahangar, D. Zhang, S.-H. Lee, C.-K. Lee, A. Khademhosseini and S. R. Shin, *ACS Appl. Mater. Interfaces*, 2019, **11**, 20615–20627.
13 X. L. Chang, P. S. Chee, E. H. Lim and W. C. Chong, *Smart Mater. Struct.*, 2019, **28**, 015024.
14 A. D. M. Shirazi, R. Faraji, M. Mehran and A. Hakimi, *Microsyst. Technol.*, 2015, **21**, 2475–2483.
15 M. D. Manrique-Juarez, F. Mathieu, A. Laborde, S. Rat, V. Shalabaeva, P. Demont, O. Thomas, L. Salmon, T. Leichle, L. Nicu, G. Molnar and A. Bousseksou, *Adv. Funct. Mater.*, 2018, **28**, 1801970.
16 T. Mulla and S.-B. Choi, *Sens. Actuators, A*, 2019, **285**, 338–347.
17 L. Breuer, J. Pilas, E. Guthmann, M. J. Schoening, R. Thoelen and T. Wagner, *Sens. Actuators, B*, 2019, **288**, 579–585.
18 P. A. Basilio, A. M. T. Rojas, E. C. Poire and L. F. Olguin, *Microfluid. Nanofluid.*, 2019, **23**, 64.
19 A. Zolfagharian, A. Z. Kouzani, S. Y. Khoo, A. A. A. Moghadam, I. Gibson and A. Kaynak, *Sens. Actuators, A*, 2016, **250**, 258–272.
20 S. W. Ng, N. Noor and Z. J. Zheng, *NPG Asia Mater.*, 2018, **10**, 217–237.
21 P. Kang, K. H. Kim, H. G. Park and S. Nam, *Light: Sci. Appl.*, 2018, **7**, 17.
22 J. L. Xue, C. G. Hu, L. X. Lv, L. M. Dai and L. T. Qu, *Nanoscale*, 2015, **7**, 12372–12378.
23 R. You, D. D. Han, F. M. Liu, Y. L. Zhang and G. Y. Lu, *Sens. Actuators, B*, 2018, **277**, 114–120.
24 Y. B. Zhu, Z. Y. Li, Z. Hao, C. Dimarco, P. Maturavongsadit, Y. F. Hao, M. Lu, A. Stein, Q. Wang, J. Hone, N. F. Yu and Q. Lin, *Light: Sci. Appl.*, 2018, **7**, 67.
25 D. D. Han, Y. L. Zhang, J. N. Ma, Y. Liu, J. W. Mao, C. H. Han, K. Jiang, H. R. Zhao, T. Zhang, H. L. Xu and H. B. Sun, *Adv. Mater. Technol.*, 2017, **2**, 1700045.

26 D. D. Han, Y. Q. Liu, J. N. Ma, J. W. Mao, Z. D. Chen, Y. L. Zhang and H. B. Sun, *Adv. Mater. Technol.*, 2018, **3**, 1800258.
27 T. Xu, X. T. Ding, C. X. Shao, L. Song, T. Y. Lin, X. Gao, J. L. Xue, Z. P. Zhang and L. T. Qu, *Small*, 2018, **14**, 1704473.
28 H. B. Jiang, Y. Liu, J. Liu, S. Y. Li, Y. Y. Song, D. D. Han and L. Q. Ren, *Front. Chem.*, 2019, **7**, 464.
29 Y. Q. Liu, Z. D. Chen, J. W. Mao, D. D. Han and X. Y. Sun, *Front. Chem.*, 2019, **7**, 461.
30 M. T. Li, M. N. Liu, Y. H. Yu, A. W. Li and H. B. Sun, *Bull. Chem. Soc. Jpn.*, 2019, **92**, 283–289.
31 H. Cheng, J. Liu, Y. Zhao, C. Hu, Z. Zhang, N. Chen, L. Jiang and L. Qu, *Angew. Chem., Int. Ed.*, 2013, **52**, 10482–10486.
32 D.-D. Han, Y.-L. Zhang, H.-B. Jiang, H. Xia, J. Feng, Q.-D. Chen, H.-L. Xu and H.-B. Sun, *Adv. Mater.*, 2015, **27**, 332–338.
33 Y. Jiang, C. G. Hu, H. H. Cheng, C. X. Li, T. Xu, Y. Zhao, H. B. Shao and L. T. Qu, *ACS Nano*, 2016, **10**, 4735–4741.
34 H. L. Gao, S. M. Chen, L. B. Mao, Z. Q. Song, H. B. Yao, H. Colfen, X. S. Luo, F. Zhang, Z. Pan, Y. F. Meng, Y. Ni and S. H. Yu, *Nat. Commun.*, 2017, **8**, 287.
35 H. Yue, J. C. Rubalcaba, Y. Cui, J. P. Fernandez-Blazquez, C. Yang and P. S. Shuttleworth, *Cellulose*, 2019, **26**, 4693–4706.
36 H. H. Cheng, Y. X. Huang, Q. L. Cheng, G. Q. Shi, L. Jiang and L. T. Qu, *Adv. Funct. Mater.*, 2017, **27**, 1703096.
37 A. M. Diez-Pascual and A. L. Diez-Vicente, *ACS Appl. Mater. Interfaces*, 2016, **8**, 17902–17914.
38 G. H. Yang, D. D. Bao, H. Liu, D. Q. Zhang, N. Wang and H. T. Li, *J. Inorg. Organomet. Polym. Mater.*, 2017, **27**, 1129–1141.
39 B. Han, Y. L. Zhang, L. Zhu, L. Ying, Z. C. Ma, Y. Q. Liu, X. L. Zhang, X. W. Cao, Q. D. Chen, C. W. Qiu and H. B. Sun, *Adv. Mater.*, 2019, **31**, 1806386.